Chapter 19

Minimizing Torque-Ripple in Inverter-Fed Induction Motor Using Harmonic Elimination PWM Technique

Ouahid Bouchhida, Mohamed Seghir Boucherit and Abederrezzek Cherifi

Additional information is available at the end of the chapter

http://dx.doi.org/10.5772/37883

1. Introduction

Vector control has been widely used for the high-performance drive of the induction motor. As in DC motor, torque control of the induction motor is achieved by controlling torque and flux components independently. Vector control techniques can be separated into two categories: direct and indirect flux vector orientation control schemes. For direct control methods, the flux vector is obtained by using stator terminal quantities, while indirect methods use the machine slip frequency to achieve field orientation.

The overall performance of field-oriented-controlled induction motor drive systems is directly related to the performance of current control. Therefore, decoupling the control scheme is required by compensation of the coupling effect between q-axis and d-axis current dynamics (Jung et al., 1999; Lin et al., 2000; Suwankawin et al., 2002).

The PWM is the interface between the control block of the electrical drive and its associated electrical motor (fig.1). This function controls the voltage or the current inverter (VSI or CSI) of the drive. The performance of the system is influenced by the PWM that becomes therefore an essential element of the system. A few problems of our days concerning the variable speed system are related to the conventional PWM: inverter switching losses, acoustical noise, and voltages harmonics (fig.2).

Harmonic elimination and control in inverter applications have been researched since the early 1960's (Bouchhida et al., 2007, 2008; Czarkowski et al., 2002; García et al., 2003; Meghriche et al., 2004, 2005; Villarreal-Ortiz et al., 2005; Wells et al., 2004). The majority of these papers consider the harmonic elimination problem in the context of either a balanced connected load or a single phase inverter application. Typically, many papers have focused

on finding solutions and have given little attention to which solution is optimal in an application context.

A pre-calculated PWM approach has been developed to minimize the harmonic ratio within the inverter output voltage (Bouchhida et al., 2007, 2008; Bouchhida, 2008, 2011). Several other techniques were proposed in order to reduce harmonic currents and voltages. Some benefit of harmonic reduction is a decrease of eddy currents and hysterisis losses. That increase of the life span of the machine winding insulation. The proposed approach is integrated within different control strategies of induction machine.

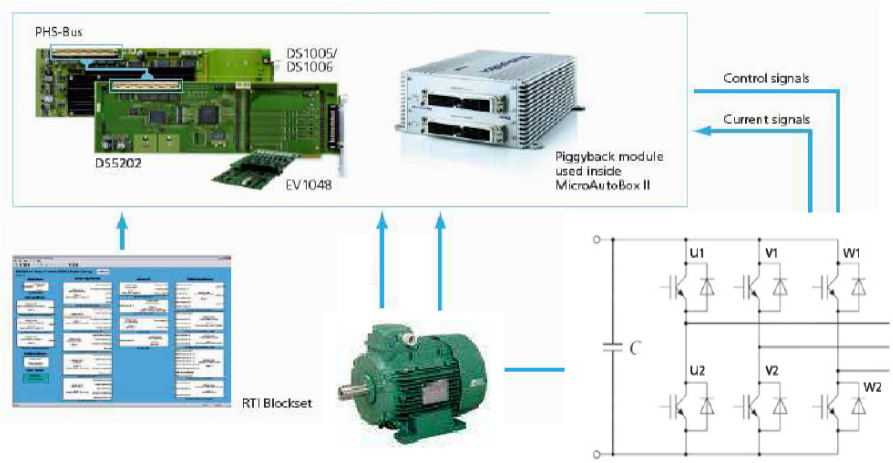

Figure 1. Global scheme of the Induction machine control

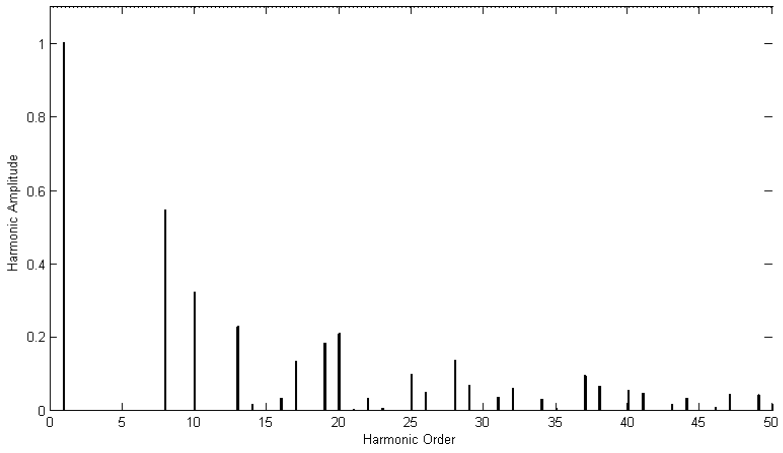

Figure 2. Harmonic spectrum of the PWM inverter output voltage.

A novel harmonic elimination pulse width modulated (PWM) strategy for three-phase inverter is presented in this chapter. The torque ripple of the induction motor can be

significantly reduced by the new PWM technique. The three-phase inverter is associated with a passive LC filter. The commutation angles are predetermined off-line and stored in the microcontroller memory in order to speed up the online control of the induction motors. Pre-calculated switching is modelled to cancel the greater part of low-order harmonics and to keep a single-pole DC voltage across the polarized capacitors. A passive LC filter is designed to cancel the high-order harmonics. This approach allows substantial reduction of the harmonic ratio in the AC main output voltage without increasing the number of switches per period. Consequently, the duties of the semiconductor power switches are alleviated. The effectiveness of the new harmonic elimination PWM technique for reducing torque-ripple in inverter-fed induction motors is confirmed by simulation results. To show the validity of our approach, DSP-based experimental results are presented.

2. New three-phase inverter model

Figure 3 shows the new structure of the three-phase inverter, with E being the dc input voltage and $U_{12\text{-}out}=V_{C1}-V_{C2}$, $U_{23\text{-}out}=V_{C2}-V_{C3}$ and $U_{31\text{-}out}=V_{C3}-V_{C1}$ are the ac output voltage obtained via a three LC filter. R represents the internal inductors resistance. Q_i and Q'_i (i=1,2,3) are the semiconductor switches. It is worth to mention that transistors Q_i and Q'_i undergo complementary switching states. V_{C1}, V_{C2} and V_{C3} are the inverter filtered output voltages taken across capacitors C_1, C_2 and C_3 respectively.

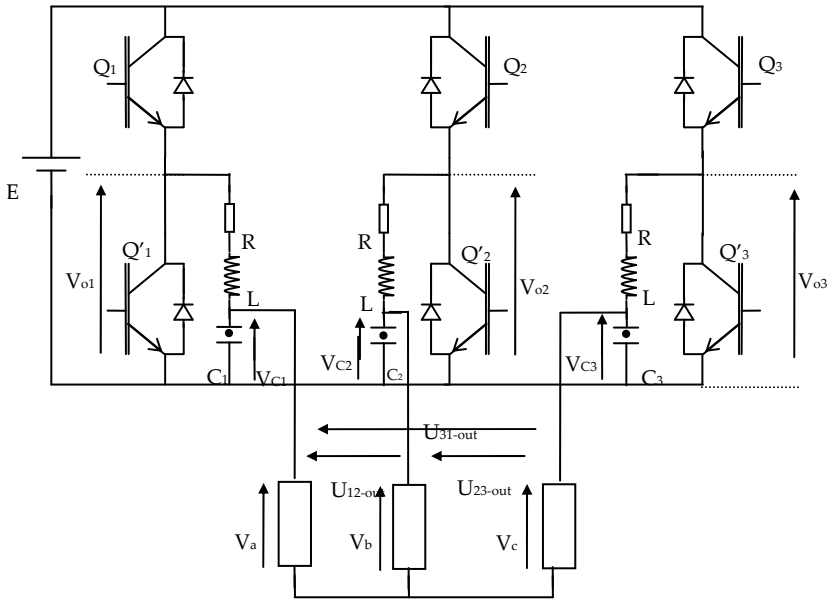

Figure 3. New three-phase inverter model.

2.1. Harmonic analysis

In ideal case, the non filtered three inverter output voltage V_{o1}, V_{o2} and V_{o3} is desired to be:

$$\begin{cases} V_{o1-ideal} = \frac{E}{2}[1+cos\,\alpha] \\ V_{o2-ideal} = \frac{E}{2}[1+cos(\alpha-\frac{2}{3}\pi)] \\ V_{o3-ideal} = \frac{E}{2}[1+cos(\alpha-\frac{4}{3}\pi)] \end{cases} \quad (1)$$

With: $\alpha=\omega t$, and ω is the angular frequency.

The relative Fourier harmonic coefficients of (1), with respect to E, are given by (2.1) or more explicitly by (2.2).

$$d_k^i = \frac{1}{E}\frac{1}{\pi}\int_{-\pi}^{+\pi} V_{oi-ideal}.cos(k\alpha)d\alpha \quad (2.1)$$

$$d_0^i = 1\,,\ d_1^i = \frac{1}{2}\,,\ d_k^i = 0\,,\ \text{for}\ k \in \left[2,\infty\right[\quad (2.2)$$

With index i is the phase number.

However, in practice, the non filtered inverter output voltage V_{o1} (V_{o2}, V_{o3}) is a series of positive impulses (see Fig. 4): 0 when Q'_1 (Q'_2, Q'_3) is on and E when Q'_1(Q'_2, Q'_3) is off, so that voltage of capacitor C_1 (C_2, C_3) is always a null or a positive value. In this case, the relative Fourier harmonic coefficients, with respect to E, are given by (3).

$$a_k^1 = \frac{2}{k\pi}\sum_{i=0}^{N_\alpha} sin\,k\alpha_i(-1)^{i+1} \quad (3)$$

Where:

k is the harmonic order

α_i are the switching angles

N_α is the number of α_i per half period

The other inverter outputs V_{o2} and V_{o3} are obtained by phase shifting V_{o1} with 2/3 π, 4/3 π, respectively as illustrated in fig. 4 for N_α=5.

The objective is to determine the switching angles α_i so as to obtain the best possible match between the inverter output V_{o1} and $V_{o1\text{-ideal}}$.

For this purpose, we have to compare their respective harmonics. A perfect matching is achieved only when an infinite number of harmonics is considered as given by (4).

$$\frac{2}{k\pi}\sum_{i=0}^{N_\alpha} sin\,k\alpha_i(-1)^{i+1} = d_k \text{, for } k \in \left[0,\infty\right[\tag{4}$$

In practice, the number of harmonics N that can be identical is limited. Thus, a nonlinear system of N+1 equations having N_α unknowns is obtained as:

$$a_k = \frac{2}{k\pi}\sum_{i=0}^{N_\alpha} sin\,k\alpha_i(-1)^{i+1} = d_k \text{, for } k \in \left[0,N\right] \tag{5}$$

To solve the nonlinear system (5), we propose to use the genetic algorithms, to determine the switching angles α_i (Bäck, 1996; Davis, 1991). The optimal switching angles family are listed in table I.

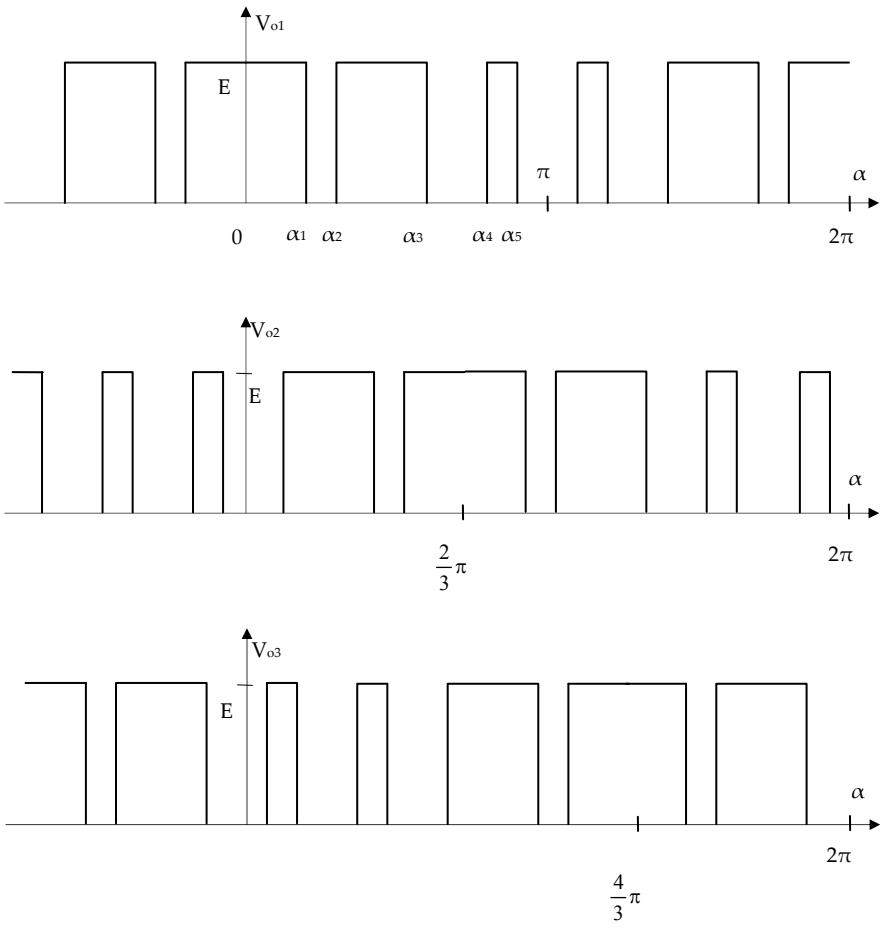

Figure 4. Inverter direct outputs representation for Nα=5.

Family	symbol	Angles (radians)	Angles (degrees)
N_α=3	α1	0.817809468	46.8570309622392
	α2	1.009144336	57.8197113723319
	α3	1.911639657	109.528884295936
N_α=5	α1	1.051000076	60.2178686227288
	α2	1.346257127	77.1348515165077
	α3	1.689593122	96.8065549849324
	α4	2.374938655	136.073961533976
	α5	2.47770082	141.961799882103
N_α=7	α1	0.52422984	30.0361573268184
	α2	0.57159284	32.7498573318965
	α3	1.14918972	65.8437208158208
	α4	1.41548576	81.1013600088678
	α5	1.66041537	95.134792939653
	α6	2.16577455	124.089741091845
	α7	2.29821202	131.677849172236
N_α=9	α1	0.43157781	24.7275870444989
	α2	0.45713212	26.1917411558679
	α3	0.70162245	40.2000051966286
	α4	0.77452452	44.3769861253959
	α5	0.96140142	55.0842437838843
	α6	1.09916539	62.9775378338511
	α7	1.21595592	69.6691422899472
	α8	1.45409688	83.3136142271409
	α9	1.64220075	94.0911720882184

Table 1. Optimal switching angles family with genetic algorithms

2.2. Dynamic LC filter behavior

Considering the inverter direct output fundamental, the LC filter transfer function is given by:

$$\bar{T} = \frac{\bar{V}_{C1}}{\bar{V}_{o1}} = \frac{1}{1 - LC\omega^2 + jRC\omega} \tag{6}$$

From (6), one can notice that for ω=0, $\bar{T}$ =1, meaning that the mean value (dc part) of the input voltage is not altered by the filter. Consequently, the inverter dc output part is entirely transferred to capacitor C_1. The same conclusion can be drawn for capacitor C_2 and C_3.

Letting $x = \omega\sqrt{LC}$ and $y = R\sqrt{\frac{C}{L}}$, the filter transfer function can rewritten as:

$$\bar{T} = \frac{\bar{V}_{C1}}{\bar{V}_{o1}} = \frac{1}{1 - x^2 + jxy} \tag{7}$$

For a given harmonic component of order k, the LC filter transfer function T_k is obtained by replacing ω with kω as:

$$\overline{T}_k = \left(\frac{\overline{V}_{C1}}{\overline{V}_{o1}} \right)_k = \frac{1}{1 - x^2k^2 + jkxy} \tag{8}$$

Assuming that the filter L and C components are not saturated, and using the superposition principle, we obtain the inverter filtered output voltages V_{C1}, V_{C2} and V_{C3}, taken across capacitors C_1, C_2 and C_3 as given by (9.1), (9.2) and (9.3) respectively:

$$V_{C1} = E(\frac{a_0}{2} + \sum_{k=1}^{N} a_k T_k \cos(k\alpha + \varphi_k)) \tag{9.1}$$

$$V_{C2} = E(\frac{a_0}{2} + \sum_{k=1}^{N} a_k T_k \cos[k(\alpha - \frac{2}{3}\pi) + \varphi_k]) \tag{9.2}$$

$$V_{C3} = E(\frac{a_0}{2} + \sum_{k=1}^{N} a_k T_k \cos[k(\alpha - \frac{4}{3}\pi) + \varphi_k]) \tag{9.3}$$

T_k and φ_k are the k^{th} order magnitude and phase components of the LC filter transfer function respectively.

Each k harmonic term of the inverter output voltage has a frequency of kω and an amplitude equal to a_kT_k, Where a_k is the amplitude of the k^{th} order harmonic of V_{o1}.

The transfer function magnitude and phase are given, respectively, by:

$$\left|\overline{T}_k\right| = T_k = \frac{1}{\sqrt{(1 - x^2k^2)^2 + y^2x^2k^2}} \tag{10}$$

$$\varphi_k = -arctan\frac{kxy}{1 - x^2k^2} \tag{11}$$

The maximum value T_{max} of T_k , obtained when $\frac{dT}{dx} = 0$, can be expressed by:

$$T_{max} = \frac{\frac{1}{y^2}}{\sqrt{\frac{1}{y^2} - \frac{1}{4}}} \tag{12}$$

In which case, (12) corresponds to a maximum angular frequency, this last is given by:

$$\omega_{max} = \frac{\sqrt{2}}{RC}\sqrt{1 - \frac{y^2}{2}} \tag{13}$$

The maximum angular frequency ω_{max} exists if, and only if, $y < \sqrt{2}$. The filter transfer function will exhibit a peak value then decreases towards zero. As consequence, the fundamental, as well as the harmonics, are amplified, this leads to undesirable situation, as illustrated in fig.5.

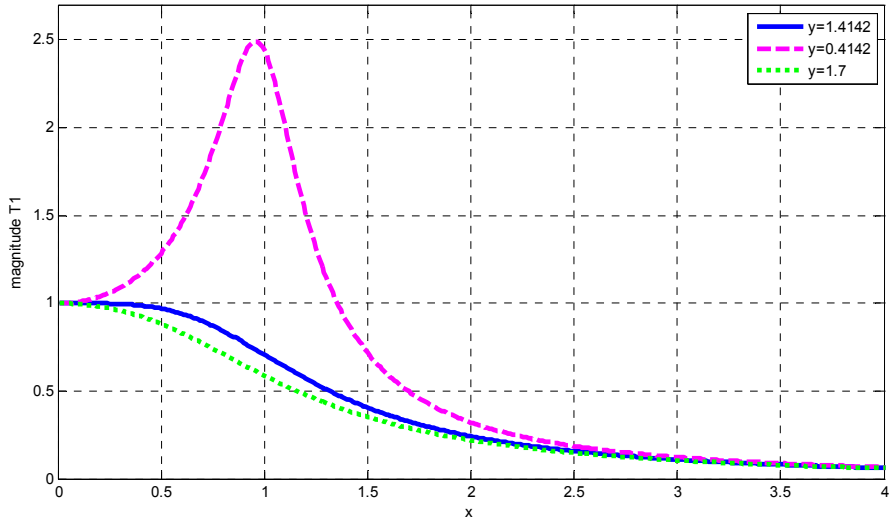

Figure 5. LC filter transfer function magnitude for the fundamental.

If (14) is satisfied, the filter transfer function will exhibit a damped behaviour.

$$y = R\sqrt{\frac{C}{L}} > \sqrt{2} \tag{14}$$

This condition matches both practical convenience and system objectives.

2.3. Harmonic rate calculation

Using (1) to (3), the non filtered inverter output voltages V_{o1}, V_{o2} and V_{o3} can be expressed as

$$V_{o1} = \frac{E}{2}(1 + \cos\omega t) + a_5 \cos 5\omega t + a_6 \cos 6\omega t + \ldots \tag{15.1}$$

$$V_{o2} = \frac{E}{2}[1 + \cos(\omega t - \frac{2}{3}\pi)] + a_5 \cos 5(\omega t - \frac{2}{3}\pi) + a_6 \cos 6(\omega t - \frac{2}{3}\pi) + \ldots \tag{15.2}$$

$$V_{o3} = \frac{E}{2}[1 + \cos(\omega t - \frac{4}{3}\pi)] + a_5 \cos 5(\omega t - \frac{4}{3}\pi) + a_6 \cos 6(\omega t - \frac{4}{3}\pi) + \ldots \tag{15.3}$$

Taking into consideration the filter transfer function, we get the expressions (16), (17) and (18) for V_{C1}, V_{C2} and V_{C3} respectively.

$$V_{C1} = \frac{E}{2}[1 + a_1.T_1.cos(\alpha + \varphi_1) + a_8.T_8.cos(8.\alpha + \varphi_8) + a_{10}.T_{10}.cos(10.\alpha + \varphi_{13}) + ... \quad (16)$$

$$V_{C2} = \frac{E}{2}[1 + a_1.T_1.cos([\alpha - \frac{2}{3}\pi] + \varphi_1) + a_8.T_8.cos(8[\alpha - \frac{2}{3}\pi] + \varphi_8) + a_{10}.T_{10}.cos(10[\alpha - \frac{2}{3}\pi] + \varphi_{10}) + ... \quad (17)$$

$$V_{C3} = \frac{E}{2}[1 + a_1.T_1.cos([\alpha - \frac{4}{3}\pi] + \varphi_1) + a_8.T_8.cos(8[\alpha - \frac{4}{3}\pi] + \varphi_8) + a_{10}.T_{10}.cos(10[\alpha - \frac{4}{3}\pi] + \varphi_{10}) + ... \quad (18)$$

Using (15), (16), (17) and (18), we get the three inverter filtered output voltages expressions as:

$$\begin{cases} U_{12-out} = E\frac{\sqrt{3}}{2}\left[a_1T_1\cos(\alpha + \beta_1) + \sum_{\substack{k=8 \\ k=3n+1 \\ k=3n+2}}^{\infty} a_kT_k\cos(k\alpha + \beta_k) \right] \\ U_{23-out} = E\frac{\sqrt{3}}{2}\left[a_1T_1\cos(\alpha + \beta_1 - \frac{2}{3}\pi) + \sum_{\substack{k=8 \\ k=3n+1 \\ k=3n+2}}^{\infty} a_kT_k\cos(k\alpha + \beta_k - \frac{2}{3}\pi) \right] \\ U_{31-out} = E\frac{\sqrt{3}}{2}\left[a_1T_1\cos(\alpha + \beta_1 - \frac{4}{3}\pi) + \sum_{\substack{k=8 \\ k=3n+1 \\ k=3n+2}}^{\infty} a_kT_k\cos(k\alpha + \beta_k - \frac{4}{3}\pi) \right] \end{cases} \quad (19)$$

with: $\beta_k = \varphi_k + \frac{\pi}{6}$.

From the precedent fig. 3, and for each lever, the equations with the currents and the voltages can be written in the following form (Bouchhida et al., 2007, 2008; Bouchhida, 2008, 2011).

- Currents equations

$$\begin{cases} \frac{dv_{C1}}{dt} = \frac{1}{C_1}(i_1 - i_{1ch}) \\ \frac{dv_{C2}}{dt} = \frac{1}{C_2}(i_2 - i_{2ch}) \\ \frac{dv_{C3}}{dt} = \frac{1}{C_3}(i_3 - i_{3ch}) \end{cases} \quad (20)$$

- Voltages equations:

$$\begin{cases} \dfrac{di_1}{dt} = (V_{o1} - R_1.i_1 - v_{C1}).\dfrac{1}{L_1} \\ \dfrac{di_2}{dt} = (V_{o2} - R_2.i_2 - v_{C2}).\dfrac{1}{L_2} \\ \dfrac{di_3}{dt} = (V_{o3} - R_3.i_3 - v_{C3}).\dfrac{1}{L_3} \end{cases} \tag{21}$$

These equations are put in following matric form:

$$\frac{d}{dt}\begin{bmatrix} v_C \\ I \end{bmatrix} = \begin{bmatrix} \mathbf{0_{3\times3}} & \dfrac{\mathbf{1}}{\mathbf{C}}\times\mathbf{I_{3\times3}} \\ -\dfrac{\mathbf{1}}{\mathbf{L}}\times\mathbf{I_{3\times3}} & -\mathbf{R}\times\mathbf{I_{3\times3}} \end{bmatrix}\begin{bmatrix} v_c \\ I \end{bmatrix} + \begin{bmatrix} -\dfrac{1}{C}\times I_{3\times3} & 0_{3\times3} \\ 0_{3\times3} & \dfrac{1}{L}\times I_{3\times3} \end{bmatrix}\begin{bmatrix} i_{ch} \\ V_o \end{bmatrix} \tag{22}$$

with : $v_C = \begin{bmatrix} v_{C1} \\ v_{C2} \\ v_{C3} \end{bmatrix}$; $I = \begin{bmatrix} i_1 \\ i_2 \\ i_3 \end{bmatrix}$; $v_o = \begin{bmatrix} v_{o1} \\ v_{o2} \\ v_{o3} \end{bmatrix}$

3. Indirect field- oriented induction motor drive

The dynamic electrical equations of the induction machine can be expressed in the d-q synchronous reference frame as:

$$\begin{cases} \dfrac{di_{ds}}{dt} = -\dfrac{1}{\sigma L_s}(R_s + R_r\dfrac{M_{sr}^2}{L_r^2})i_{ds} + \omega_s i_{qs} + \dfrac{M_{sr}R_r}{\sigma L_s L_r^2}\psi_{dr} + \dfrac{M_{sr}}{\sigma L_s L_r}\psi_{qr}\omega_r + \dfrac{1}{\sigma L_s}V_{ds} \\ \dfrac{di_{qs}}{dt} = -\omega_s i_{ds} - \dfrac{1}{\sigma L_s}(R_s + R_r\dfrac{M_{sr}^2}{L_r^2})i_{qs} - \dfrac{M_{sr}}{\sigma L_s L_r}\psi_{dr}\omega_r + \dfrac{M_{sr}R_r}{\sigma L_s L_r^2}\psi_{qr} + \dfrac{1}{\sigma L_s}V_{qs} \\ \dfrac{d\psi_{dr}}{dt} = \dfrac{M_{sr}R_r}{L_r}i_{ds} - \dfrac{R_r}{L_r}\psi_{dr} + \omega_g\psi_{qr} \\ \dfrac{d\psi_{qr}}{dt} = \dfrac{M_{sr}R_r}{L_r}i_{qs} - \omega_g\psi_{dr} - \dfrac{R_r}{L_r}\psi_{qr} \end{cases} \tag{23}$$

$$\frac{d\Omega_r}{dt} = -\frac{f}{j}\Omega_r - \frac{1}{j}(C_{em} - C_r) \tag{24}$$

$$\Omega_r = \frac{\omega_r}{p} \tag{25}$$

$$C_{em} = p\frac{M_{sr}}{L_r}(\psi_{dr}i_{qs} - \psi_{qr}i_{ds}) \tag{26}$$

Where:

V_{ds} , V_{qs} : d-axis and q-axis stator voltages;

i_{ds} , i_{qs} : d-axis and q-axis stator currents;

ψ_{dr} ,ψ_{qr} : d-axis and q-axis rotor flux linkages;

R_s , R_r : stator and rotor resistances;

L_s , L_r : stator and rotor inductances;

M_{sr} : mutual inductance

ω_s ,ω_r : electrical stator and rotor angular speed

ω_g : slip speed ωg=(ωs-ωr)

Ω_r : mechanical rotor angular speed

C_r , C_{em} : external load torque and motor torque

j , f : inertia constant and motor damping ratio

p : number of pole pairs

σ : leakage coefficient, ($\sigma = 1 - \frac{M_{sr}^2}{L_s L_r}$)

Equation (23) represents the dynamic of the motor mechanical side and (26) describes the electromagnetic torque provided on the rotor. The model of a three phase squirrel cage induction motor in the synchronous reference frame, whose axis d is aligned with the rotor flux vector, ($\psi_{dr}=\psi_r$ and $\psi_{qr}=0$), can be expressed as:

$$\frac{di_{ds}}{dt} = -\gamma i_{ds} + \omega_s i_{qs} + \frac{K}{T_r}\psi_{dr} + \frac{1}{\sigma L_s}V_{ds} \tag{27}$$

$$\frac{di_{qs}}{dt} = -\omega_s i_{ds} - \gamma i_{qs} - p\Omega K\psi_{dr} + \frac{1}{\sigma L_s}V_{ds} \tag{28}$$

$$\frac{d\psi_{dr}}{dt} = \frac{M_{sr}}{T_r} i_{ds} - \frac{1}{T_r}\psi_{dr} \tag{29}$$

$$\frac{d\dot{\psi}_{qr}}{dt} = \frac{M_{sr}}{T_r} i_{qs} - (\omega_s - p\Omega)\psi_{dr} \tag{30}$$

$$\frac{d\dot{\Omega}}{dt} = \frac{pM_{sr}}{JL_r}(\psi_{dr} i_{qs}) - \frac{C_r}{J} - f\,\Omega \tag{31}$$

With: $T_r = \frac{L_r}{R_r}$, $K = \frac{M_{sr}}{\sigma L_s L_r}$, $\gamma = \frac{R_s}{\sigma L_s} + \frac{R_r M_{sr}^2}{\sigma L_s L_r^2}$.

The bloc diagram of the proposed indirect field-oriented induction motor drive is shown in fig.6. Speed information, obtained by encoder feedback, enables computation of the torque reference using a PI controller. The reference flux is set constant in nominal speed. For higher speeds, rotor flux must be weakened.

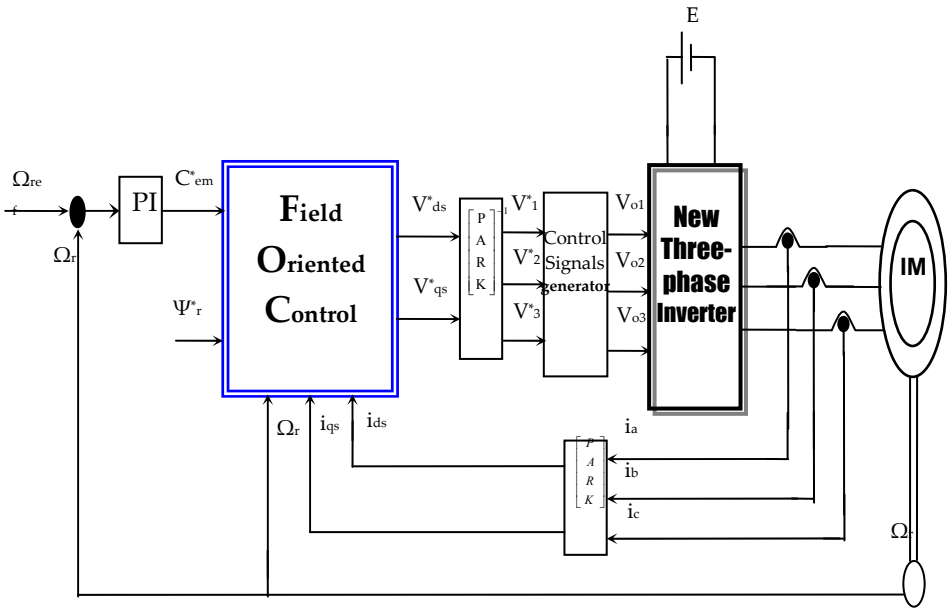

Figure 6. Block diagram of the proposed indirect field oriented induction motor drive system.

4. Simulation results

To demonstrate the performance of a new tree-phase inverter, we simulated three filtered inverter output voltages. Two frequency values are imposed on the inverter, starting with a frequency of 50 Hz, then at time t=0.06(s) the frequency is changed to 60Hz. The three filtered inverter output voltages are illustrated in (figure 7.a) which clearly shows that the three voltages are perfectly sinusoidal and follow the ideal values with a transient time of

0.012(s). The harmonic spectrum of the filtered output voltage is shown in (figure 7.b). In order to compare the performance of the new three-phase inverter with the conventional PWM inverter, the output voltage of the latter, where a modulation index of 35 was used, is shown in (figure 8.a) and its harmonic spectrum is presented in (figure 8.b).

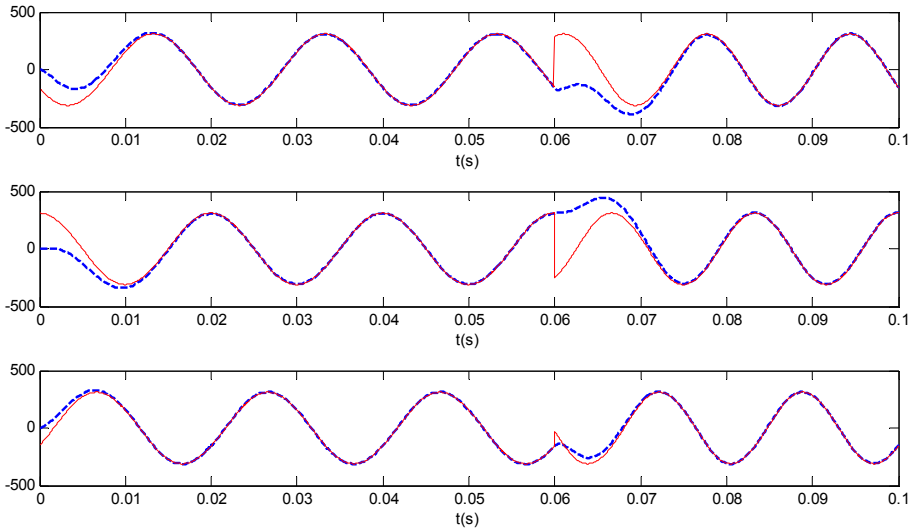

('---' filtered output voltage) ('—' ideal output voltage)

(a)

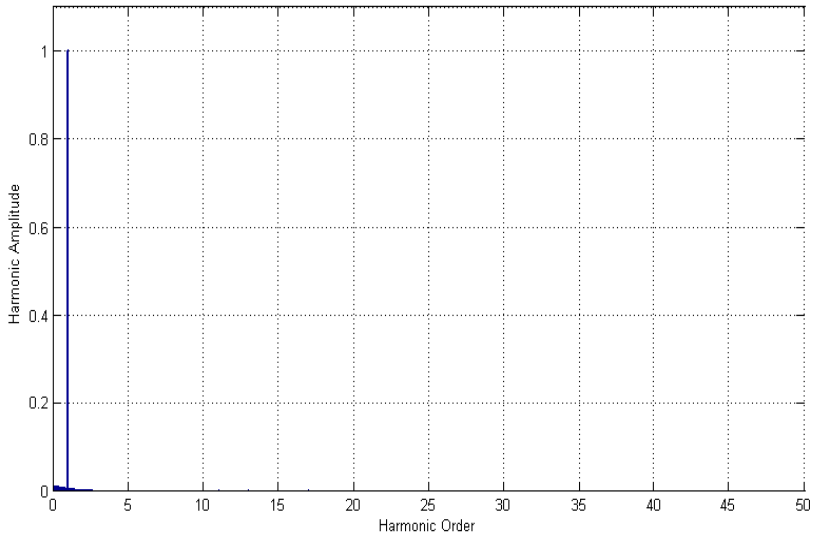

(b)

Figure 7. (a) Three filtered inverter outputs voltages.(b) Harmonic spectrum of the filtered output voltage.

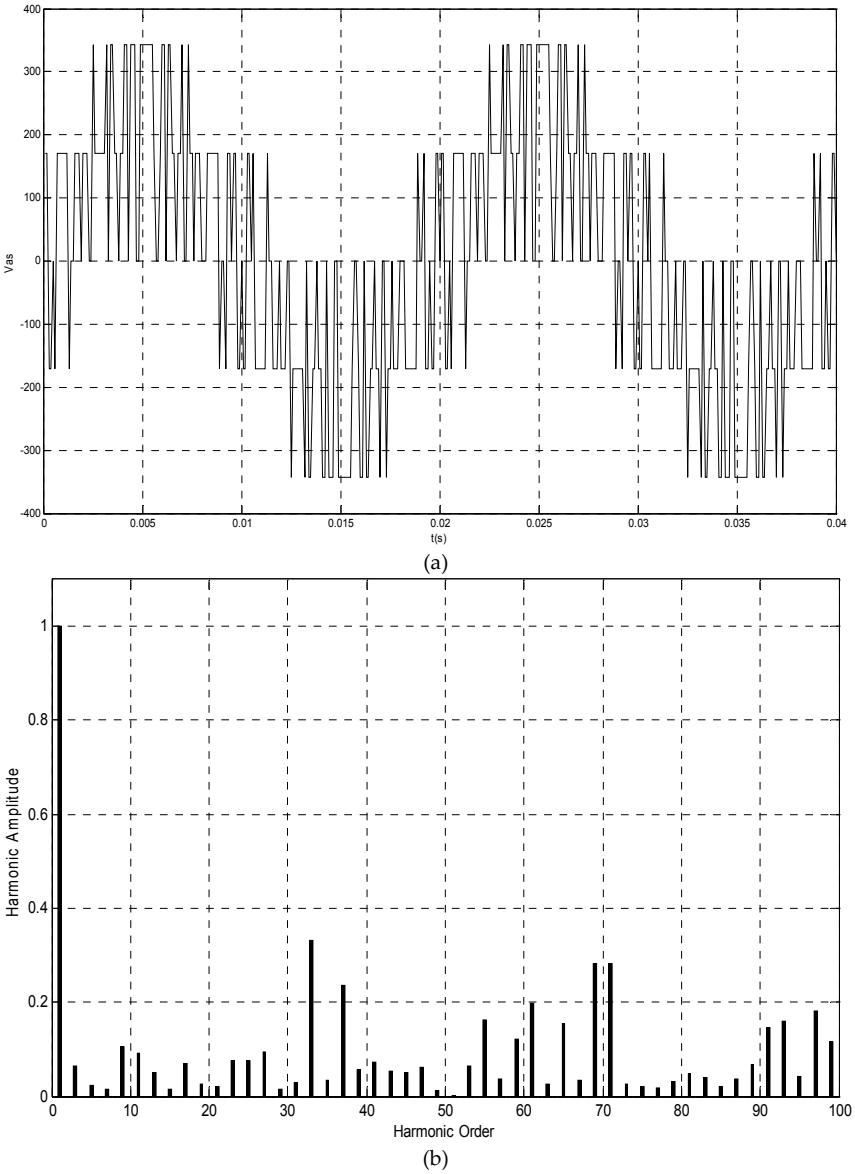

Figure 8. (a) PWM inverter output voltage (b) Harmonic spectrum of thePWM inverter output voltage.

We carried out two simulations of the field-oriented control for induction motor drives with speed regulation using the new structure of the three phase inverter in the first simulation (figure 9.a) and the conventional PWM (figure 9.b) inverter in the second simulation. The instruction speed is set to 100 (rad/sec) for both simulations. During the period between 1.3(s) and 2.3(s), a resistive torque equal to 10 (N.m) (i.e the nominal torque) is applied.

In order to illustrate the effectiveness of the proposed inverter, the torque response obtained by using the proposed and the conventional PWM inverters are shown in (figure 10.a) and (figure 10.b), respectively. The obtained results clearly show that the conventional PWM inverter generates more oscillations in the torque than the proposed structure (figure 11). Moreover, the switching frequency of the proposed inverter is dramatically reduced (see (figure 12.a)) when compared to its counterpart in the conventional PWM inverter (see figure 12.b). Therefore, the proposed inverter gives a better dynamic response than the conventional PWM inverter.

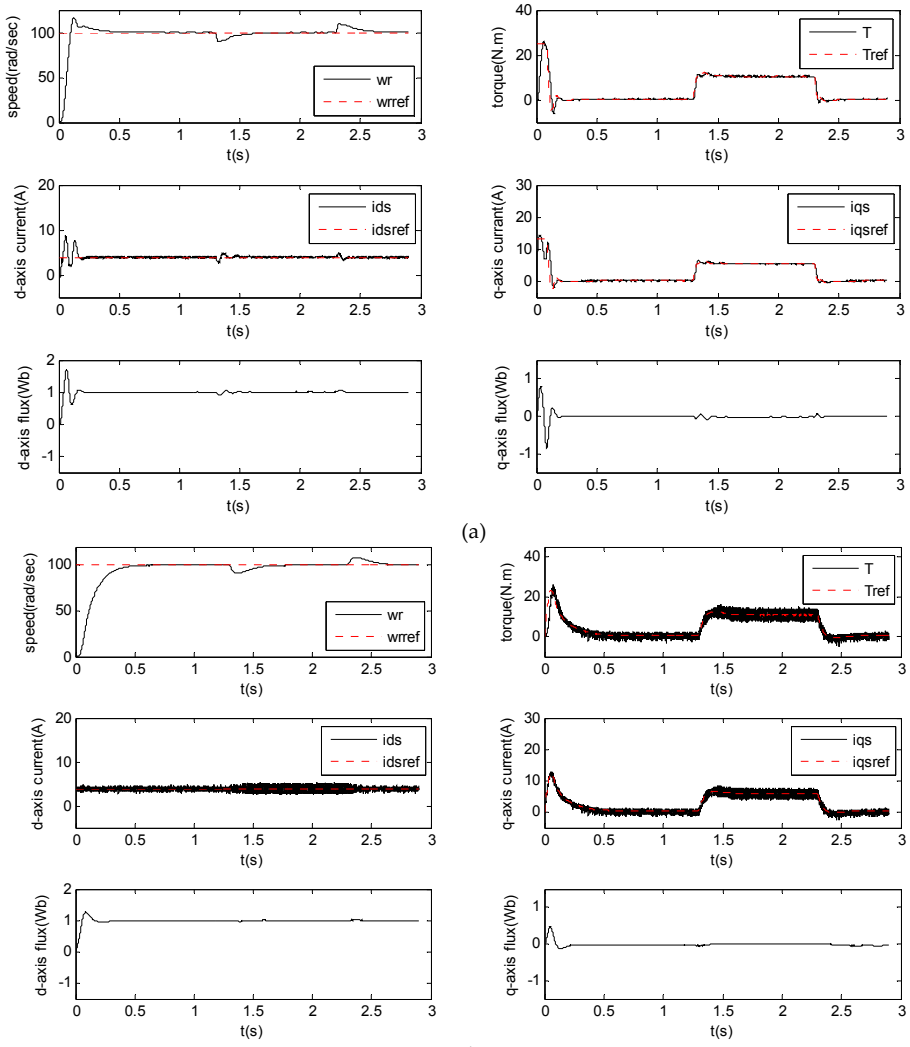

Figure 9. (a) Simulation results of the indirect field-oriented control for proposed inverters (b) Simulation results of the indirect field-oriented control for conventional PWM inverters

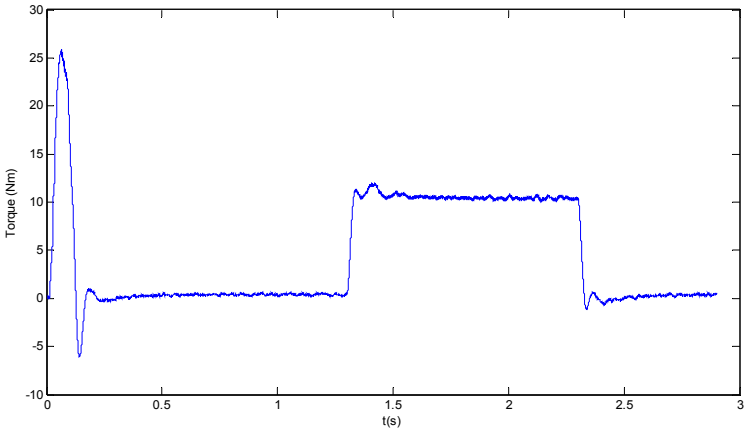

(a)

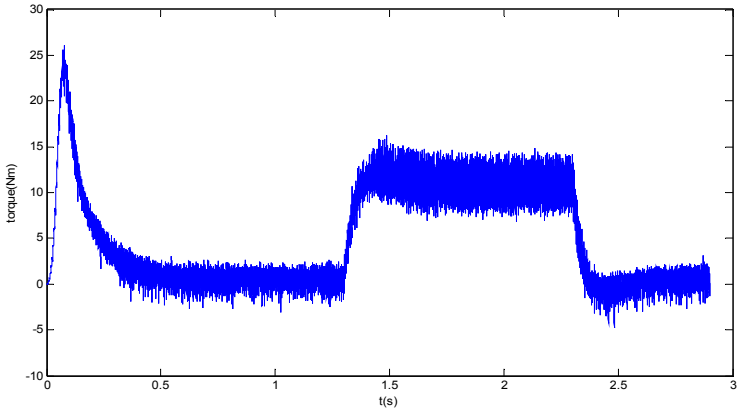

(b)

Figure 10. (a) Torque response for proposed inverters (b)Torque response for conventional PWM inverters

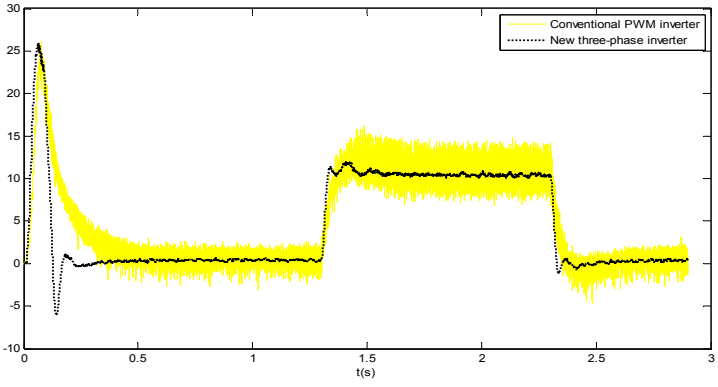

Figure 11. Torque response for proposed and conventional PWM inverters

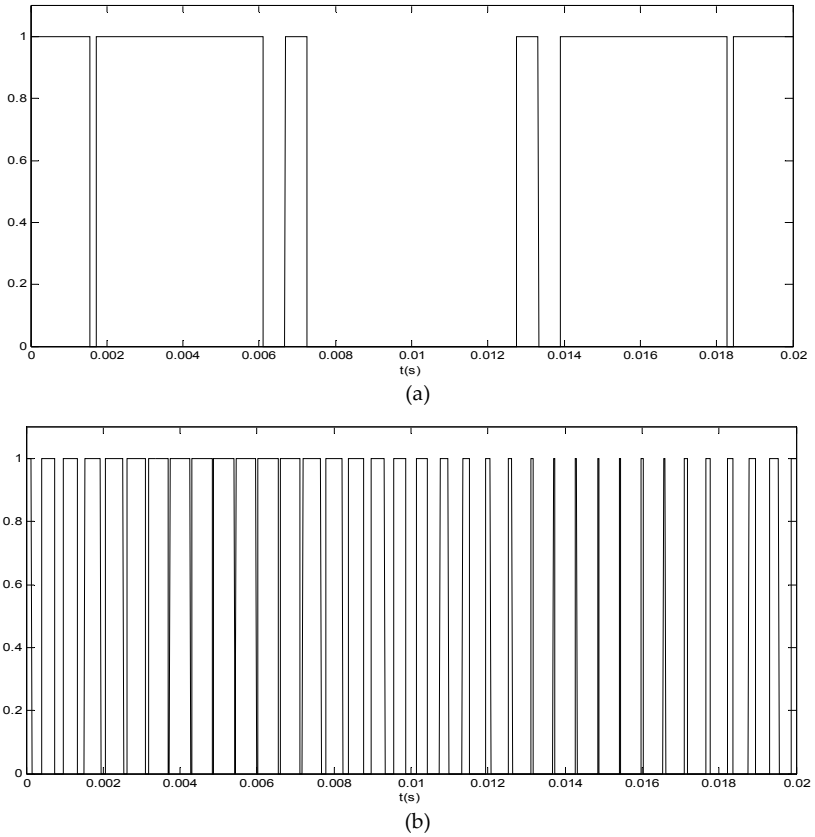

Figure 12. (a) Switching frequency for proposed inverters (b) Switching frequency for conventional PWM inverters

5. Experimental setup

The experimental setup was realized based on the DS1103 TMS320F240 dSPACE kit (dSPACE, 2006a, 2006b, 2006c, 2006d, 2006e). Figure 13 gives the global scheme of the experimental setup. This kit allows real time implementation of inverter and induction motor IM speed drive, it includes several functions such as Analog/Digital converters and digital signal filtering. In order to run the application the control algorithm must be written in C language. Then, we use the RTW and RTI packages to compile and load the algorithm on processor. To visualize and adjust the control parameters in real time we use the software control-desk which allows conducting the process by the computer.

The novel single phase inverter structure for pre-calculated switching is based on the use of IGBT (1000V/25A) with 10 kHz as switching frequency. The switching angles are predetermined off-line using Genetic Algorithms and stored in the card memory in order to speed up the programme running. The non-filtered inverter output voltages are first

designed in Simulink/Matlab, then, the Real-Time Workshop is used to automatically generate optimized C code for real time application. Afterward, the interface between Simulink/Matlab and the Digital Signal Processor (DSP) (DS1103 of dSPACE) allows the control algorithm to be run on the hardware.

The master bit I/O is used to generate the required 2 gate signals, and a several Analog-to-Digital converters (ADCs) are used for the sensed line-currents, capacitors voltage, and output voltage. An optical interface board is also designed in order to isolate the entire DSP master bit I/O and ADCs. The block diagram of the experimental plant is given in figure 14

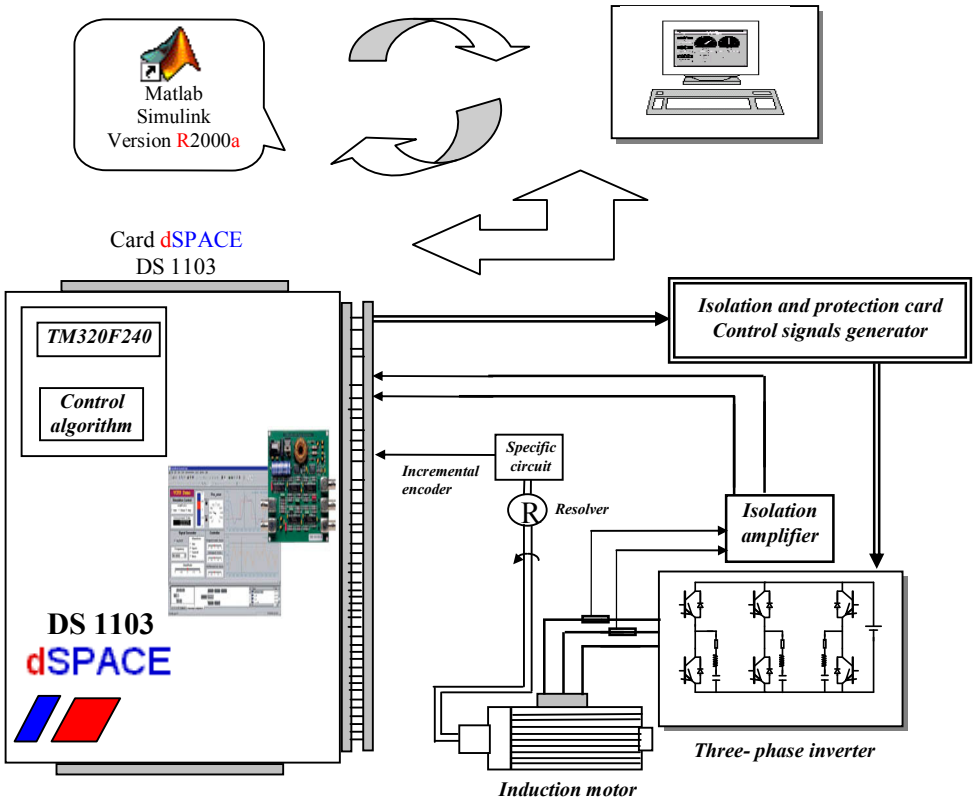

Figure 13. Global scheme of the experimental setup

6. Experimental evaluation

Figure 15 shows the experimental filtered inverter output voltage (V_{C1}-V_{C2}) for frequency value equal 50 Hz. The filtered inverter output voltage is perfectly sinusoidal. The experimental result in Figure 16 shows the torque response obtained by using the proposed PCPWM inverter: during the period between 0.65 sec and 1.95 sec, a load torque equal to 13 (N.m) is applied. The torque ripple of the induction motor is dramatically reduced.

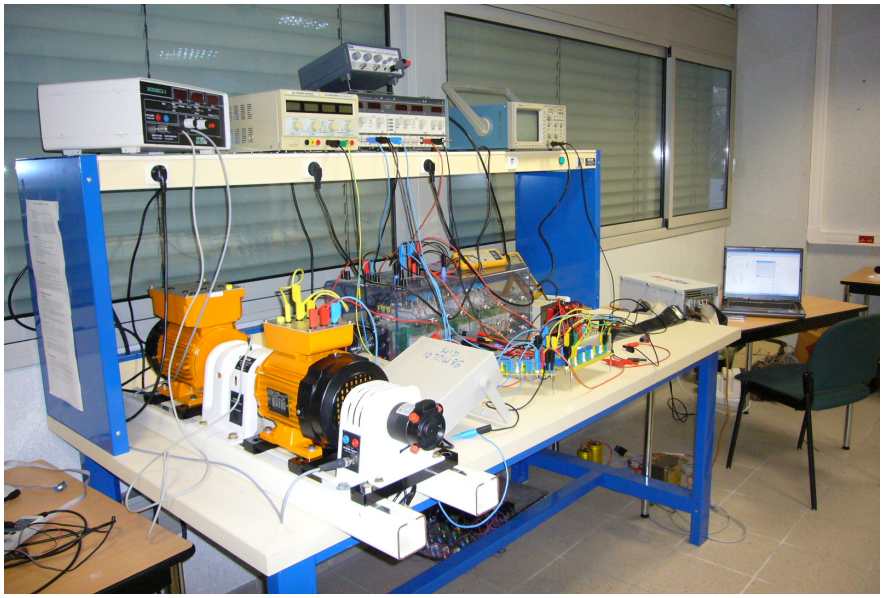

Figure 14. Snapshot of the laboratory experimental setup

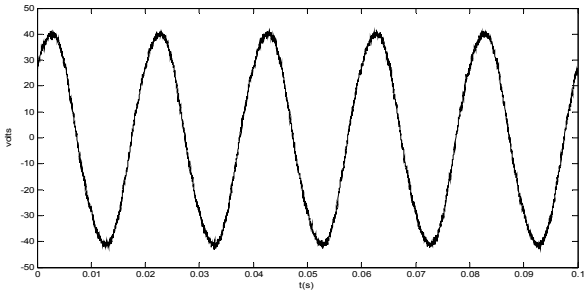

Figure 15. Experimental inverter filtered output voltage.

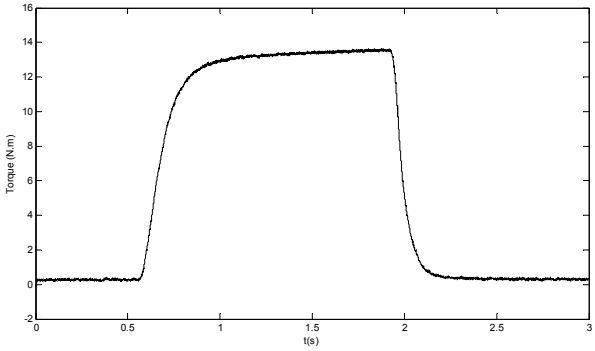

Figure 16. Experimental torque response for proposed PCPWM inverters

Moreover, as shown in Figure 17, the experimental switching frequency of the proposed PCPWM inverter is very less compared to the conventional PWM inverter one Figure 18. As a consequence, the proposed inverter provides higher dynamic response than the conventional PWM inverter in vector controlled induction motor applications.

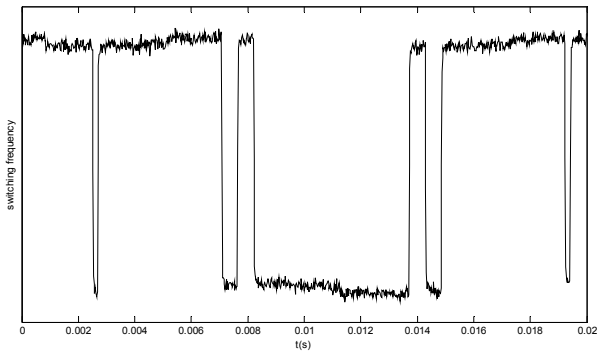

Figure 17. Experimental switching frequency for proposed PCPWM inverters

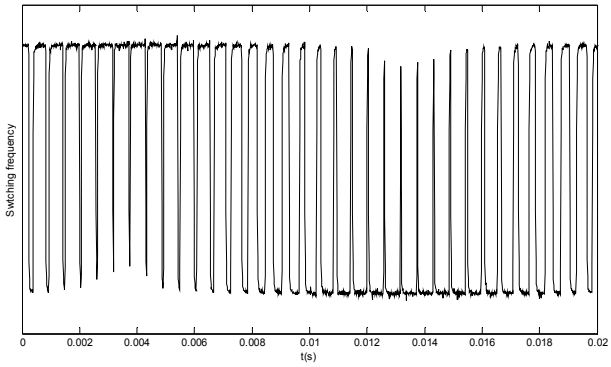

Figure 18. Experimental switching frequency for conventional PWM inverters

7. Conclusion

A three-phase inverter model was developed by combining pre-calculated switching angles and a passive filter to eliminate inverter output harmonics. The inverter model needs a nonlinear system of equations for the switching angles computation. The proposed inverter model succeeds to substantially reduce the harmonics while using polarized capacitors. The reduced number of switching angles provides more reliability and increases system components life time. Moreover, the proposed inverter design and control simplicity could be used as a cost effective solution to harmonics reduction problem. The torque ripple of the induction motor is dramatically reduced by the PCPWM inverter. The global scheme of the experimental setup has been implemented. The obtained experimental results exhibit good matching with the theoretical values. It is shown that the proposed PCPWM has better tracking performance as compared with the conventional PWM.

Author details

Ouahid Bouchhida
Université Docteur Yahia Farès de Médéa, Département Génie Electrique, Algérie

Mohamed Seghir Boucherit
Ecole Nationale Polytechnique, Département Génie Electrique, Algérie

Abederrezzek Cherifi
IUT Mantes-en-Yvelines, France

Appendix

The squirrel cage induction motor data are:

Symbol	Quantity	Value
P_n	Rated power	1.5 KW
V_n	Rated line voltage	220/380 V
C_n	Rated load torque	10 Nm
P	No. of pole pair	2
R_s	Stator resistance	5.62 Ω
R_r	Rotor resistance	4.37 Ω
M_{sr}	Mutual inductance	0.46 H
L_s	Stator leakage inductance	0.48 H
L_r	Rotor leakae inductance	0.48 H
I_n	Rated current	6.4/3.7 A
Ω_n	Motor speed	1480 tr/min
f	Viscosity coefficient	0.001136 N.m.s/rd
J	Moment of inertia	0.0049 kg.m²
C_1, C_2, C_3	Capacitance	10 mF
L	Inductance	0.5 mH
R	Internal inductor resistance	0.5Ω

8. References

Bäck, T. (1996). *Evolutionary Algorithms in Theory and Practice*, Oxford University Press, 1996

Bouchhida, O.; Cherifi, A. & Boucherit, M.S. (2007). Novel harmonic elimination PWM Technique for reducing Torque–Ripple in Inverter-fed Induction motor. *Archives of Electrical Engineering (AEE)*, Vol. 56, No.3-4, (Mar. 2007), 197-212.

Bouchhida, O.; Benmansour, K.; Cherifi, A. & Boucherit, M.S. (2008). Low switching-frequency and novel harmonic elimination for three-phase inverter', *Proceedings of the Fifth International Multi-Conference on Systems, Signals and Devices SSD08, IEEE*, Philadelphia University Amman Jordan, July 2008.

Bouchhida, O. (2008). *Contribution à l'Optimisation de Structure des Convertisseurs pour la Commande des Machines Asynchrones: Réalisation expérimentale*. thèse de Doctorat, Ecole Nationale polytechnique ENP d'Alger, Algérie

Bouchhida, O. (2011). *Etude et Optimisation des Performances d'Onduleur Monophasé et Triphasé à Commutation Pré-Calculée*. Habilitation Universitaire, Université Saad D'hleb Blida, Algérie

Czarkowski, D.; Chudnovsky, D.; Chudnovsky, G. & Selesnick, I. (2002). Solving the optimal PWM problem for Single-phase inverters. *IEEE Transactions Circuits Syst*. I, Vol. 49, (April 2002), 465-475

Davis, L. (1991). *The Handbook of Genetic Algorithms*, Van Nostrand & Reinhold, 1991

dSPACE (2006a). *DS1103 PPC Controller Board, Feature, Realise 5.1*, dSPACE digital signal processing and control engineering, Germany

dSPACE (2006b). *How to implement user-specific functions on the DS1103 slave DSP (TMS320F240).* dSPACE digital signal processing and control engineering GmbH, Germany

dSPACE (2006c). *DS1103 PPC Controller Board, Hardware Installation and Configuration, Realise 5.1*, dSPACE digital signal processing and control engineering, Germany

dSPACE (2006d). *DS1103 PPC Controller Board RTI Reference, Realise 5.1*, dSPACE digital signal processing and control engineering, Germany

dSPACE (2006e). *DS1103 PPC Controller Board RTLib Reference, Realise 5.1*, dSPACE digital signal processing and control engineering, Germany

García, O.; Martínez-Avial, M.D.; Cobos, A.; Uceda, J.; González, J. & Navas, A. (2003). Harmonic reducer converter. *IEEE Transactions on Industrial Electronics*, Vol. 50, No. 2, (April 2003), 322–327

Jung, J. & Nam, K. (1999). A dynamic decoupling control scheme for high speed operation of induction motors. *IEEE Transaction on Industrial Electronics, V*ol.46, No. 1, (Feb 1999), 100–110.

Lin, F.J.; Wai, R.J.; Lin, C.H.; & Liu, D.C. (2000). Decoupling stator-flux oriented induction motor drive with fuzzy neural network uncertainly observer. *IEEE Transaction on Industrial Electronics*, Vol.47, No.2, (Apr 2000), 356–367.

Meghriche, K.; Chikhi, F. & Cherifi, A. (2004). A new switching angle determination method for three leg inverter, *Proceedings of International IEEE Mechatronics and Robotics MechRob-2004*, 378–382, Aachen, Germany, September 2004

Meghriche, K.; Mansouri, O. & Cherifi, A. (2005). On the use of pre-calculated switching angles to design a new single phase static PFC inverter, *Proceedings of the 31st IEEE IECON'05*, 906–911, Raleigh North-Carolina, November 2005.

Suwankawin, S. ; & Sangwongwanich, S. (2002). A speed sensorless IM drive with decoupling control and stability analysis of speed estimation. *IEEE Transaction on Industrial Electronics*, Vol. 49, No. 2, (Apr 2002), 444–455.

Villarreal-Ortiz, R.A.; Hernández-Angeles, M.; Fuerte-Esquivel, C.R. & Villanueva-Chávez, R.O. (2005). Centroid PWM technique for inverter harmonics elimination. *IEEE Transactions on Industrial Electronics*, Vol. 20, No. 2, (April 2005), 1209–1210

Wells, J.R.; Nee, B.M.; Chapman, P.L. & Krein, P.T. (2004). Optimal Harmonic elimination control, *Proceedings of the 35th Annual IEEE Power Electronics Specialists Conference*, 4214-4219, Aachen, Germany, 2004.